

Magnetic hose: Routing and Long-distance Transportation of Magnetic Fields

Carles Navau¹, Jordi Prat-Camps¹, Oriol Romero-Isart²,
J. Ignacio Cirac², and Alvaro Sanchez¹

¹Departament de Física, Universitat Autònoma de Barcelona,
08193 Bellaterra, Barcelona, Catalonia, Spain

²Max-Planck-Institut für Quantenoptik, Hans-Kopfermann-Strasse 1, D-85748, Garching, Germany

Magnetism is a fundamental interaction shaping our physical world, at the basis of technologies such as magnetic recording or energy generation. Unlike electromagnetic waves, which can be routed and transmitted with waveguides to long distances, magnetic fields rapidly decay with distance. Here we present the concept, design, and properties of a magnetic hose which enables to transfer the static magnetic field generated by a source to an arbitrary distance, and along any given trajectory. We experimentally demonstrate the field transmission through the simplest hose realization using a superconducting shell with a magnetic core. We discuss possible application of magnetic hoses to harness quantum systems by addressable magnetic fields, in the context of quantum information processing.

The impact of magnetism in science [1] is limited by an apparently insurmountable restriction: magnetic fields rapidly decay with the distance from the sources. Our goal in this work is to design a magnetic hose that can route static magnetic fields from their sources (e. g. a magnet) to arbitrary long distances along a desired path, and to come up with a feasible realization. Magnetic field transmission is routinely used in technologies such as transformers, typically using a ferromagnetic (FM) material with high magnetic permeability μ . However, this only works for small distances, because the transmitted field rapidly decays with distance (see figure S1 in the Supplementary Material). Moreover, even though superconductors (SCs) expel magnetic field, they cannot be used to transmit magnetic field lines through a hollow superconductor tube, because the field inside a hollow SC tube decays exponentially (see Supplementary Material Section VI and [2]). Thus, transmission to arbitrary distances has never been achieved for static fields. A completely different approach is presented in this work. We will proceed in several steps, starting from mathematically exact but unfeasible schemes, based on transformation optics, and ending with feasible proposals that will be experimentally confirmed.

Transformation optics [1, 3, 4, 6] allows subwavelength control of electric and magnetic field lines, rather than rays [6]. This has enabled realizing invisibility cloaks [1, 7, 8], perfect lenses [9], and waveguides operating in the subwavelength regime [10–12]. Particularly powerful is the application to static fields like our present case, where one can literally get inside the (infinite) wavelength [13–20]. We find an exact solution for our goal using transformation optics. An infinitely wide slab of thickness t made of a homogenous material with $\mu_{\parallel} = \infty$ along the thickness and $\mu_{\perp} = 0$ along the width exactly transports the magnetic field from the lower surface of the slab to the upper surface (see Figs. 1A and 1B for the case of a dipolar source and also Supplementary Material Sect. II). The slab has other remarkable properties. First, magnetic induction \mathbf{B} is vertical and magnetic field \mathbf{H} horizontal in the material volume; because \mathbf{B} is perpendicular to \mathbf{H} , the material has zero magnetic energy [20]. Second, \mathbf{B} and \mathbf{H} -and thus magnetic energy- are not modified in the region containing the sources. The magnetic energy originally in the material volume is thus transferred to the other end. This is valid for any magnetic source and for any slab thickness t . Obviously, this ideal design is not feasible, both because the slab is infinitely wide and because no materials exist with such extreme anisotropy.

Let us address the two difficulties separately. First, we numerically calculate (see Supplementary Material) the magnetic field response of a cylindrical piece of material with finite radius R , length L and $\mu_{\rho} = 0$ and $\mu_z = \infty$, with a vertically-aligned magnetic dipole at a distance d below its bottom end (inset in Fig. 1C). We show in Fig. 1C the maximum vertical field B_z (always found at $\rho = 0$) at a distance d above the top end as a function of L and R . B_z decreases only slightly when the material length increases and rapidly saturates to a certain value that depends on R . It can be demonstrated (based on magnetic poles, see Supplementary Material Sect. III) that this saturated value is not zero, so a part of the magnetic field is always transported through the hose to arbitrary distances. For $R = 4d$ and lengths up to $L = 10d$ the material transports the field from one end of the hose to the other, similarly to the ideal infinite slab. This property is approximately maintained even for radii as small as $R = 2d$.

Now we have a magnetic hose with finite radius, but still requires non-existing materials. One way to solve this is by using a similar strategy as that for magnetic cloaks and concentrators [15, 20]. The extreme anisotropic medium with $\mu_{\rho} = 0$ and $\mu_z = \infty$ can be approximated using only existing isotropic materials: a series of n alternated superconducting (ideally with $\mathbf{B} = 0$ in their volume) and soft ferromagnetic (ideally with $\mathbf{H} = 0$) concentric cylindrical layers. Ferromagnetic parts provide a large vertical permeability and the alternated superconductors prevent radial \mathbf{B} components. In Fig. 2 we show calculated results for several

discretized versions of the magnetic hose into n concentric cylindrical shells, half of them superconducting and half ferromagnetic. The field of the dipole, located at one end of the hose, transferred at the opposite end tends to the ideal behavior with increasing n . More than 90% of the transmission is achieved with $n=20$. Remarkably, even with a simple bilayer ($n=2$) the transmission can be as high as 75% (as in Fig. S1). In this bilayer scheme the SC has to be the outer layer, surrounding the FM, in order to prevent the field lines attracted by the inner FM core to leak outside through the lateral surface.

In view of its excellent performance, we concentrate hereafter on the simplest hose discretization, a SC shell with a FM core. In Figs. 3A, 3D, and 3E we show calculations illustrating the routing of the magnetic field of a dipolar source through hoses with different topologies with open and closed exits; many combination of sources, branching geometries, and open and closed ends can be made following these examples. Results provide a clear verification of the capabilities of the magnetic hose -even in its simplest discretization- for routing and long-distance transportation of magnetic fields (see Supplementary Material Section VII), something that cannot be obtained with only the FM or the SC (see a comparison with a FM cylinder in figure S1 of the Supplementary Material).

For the case of closed hoses (as in Figs. 3C and 3F), we have validated the numerical results, from first principles, by analytically solving magnetostatic Maxwell equations with the boundary conditions that \mathbf{B} is zero in the SC and the scalar magnetic potential is constant in the FM (see Supplementary Material Section VI). We find that the field of the dipolar source with magnetic moment m in the left branch of Fig. 3C is in part transferred towards the air gap (right), and builds up there according to the expression

$$B_z = \frac{\mu_0 m}{2\pi R^2} \frac{1}{l_s + l_a}. \quad (1)$$

R is the radius of the FM core, μ_0 the vacuum permeability, and l_s , and l_a the lengths of the source and air gaps, respectively. Eq. (1) shows that the field in the whole air gap is uniform and vertical [21], and does not depend on the hose length.

We have experimentally confirmed the magnetic field transmission through a SC tube with a FM core. We used a high-temperature superconducting hollow tube and a soft magnetic cylinder with large permeability and very low coercivity (see Supplementary Material). The experiment consisted of placing a coil next to the edge of the SC tube with the FM inside (Fig. 4B). We fed a dc current in the coil and measured the magnetic field on the exterior of the SC tube by a Hall probe. Because only a SC shell shorter than the inner FM core was available to us, we checked magnetic-field transmission at the lateral surface of the SC and not at its end. We show in Fig. 4A the measured radial component of B -field on the surface of the SC, B_r , at several distances z from the edge of the superconducting tube, in three different experiments. First we measured the coil only (green in Fig. 4A); data indicate the natural decay of field with distance. When the FM cylinder was placed (red), the value of B_r increased, because of the FM magnetic response. When the SC tube surrounded the FM cylinder (blue), an overall decrease of B_r occurred (resulting from the shielding effect of the SC tube), except at a distance $z \simeq 35$ mm, where B_r presented a very large value. We found that this corresponded to the presence of a crack in the tube (difficult to be seen by the naked eye). The value of this field escaping through the hole was much larger not only than the bare field of the coil but also than the field with the FM alone. Actually, the measured value of B_r at $z \simeq 35$ mm was around 0.8mT, a substantial part of the maximum field created by the coil at its center, $B_z(z=0)=1.3$ mT. It is thus seen that the magnetic field has been guided through the SC-FM magnetic hose from the coil source up to the crack point, where it escapes to the exterior of the hose, verifying the theory.

Since we deal with static fields, associated with an infinite wavelength, these ideas can be implemented at any scale [6, 13, 17, 20]. This hints at the possibility of miniaturizing the magnetic hose to the nanoscale. Such a magnetic nanohose could be used as a new tool to harness quantum systems, as required, for instance, in quantum information processing [22]. In particular, such a device would permit to address, control, and manipulate the internal state of individual quantum systems, even if they are separated by distances of the order of few tens of nanometers, where optical methods are no longer available. This could be particularly relevant in the context of Nitrogen-vacancy (NV) color defect centers in a diamond nanocrystal [23], which have recently been identified as promising systems for the implementation of quantum information processors [24], or quantum repeaters [25]. So far, we have just considered the transmission of classical magnetic fields. One could also envision a similar system as the one considered here to couple distant quantum systems magnetically, allowing to separate them by relatively long distances and still strongly interact with each other (see Fig. 4C). This would provide us with a very powerful alternative to existing methods that directly couple NV centers at the quantum level [26]. The characterization of such a system, however, requires a full quantum treatment, something that is out of the scope of the present work.

Acknowledgements

We thank Peter Zoller for discussions and Vacuumschmelze for providing the ferromagnetic cylinder. We acknowledge funding from the EU projects AQUTE, and Spanish Consolider NANOSELECT (CSD2007-00041) and MAT2012-35370 projects. JPC acknowledges a FPU grant from Spanish Government (AP2010-2556).

[1] J. M. D. Coey, *Magnetism and Magnetic Materials*, Cambridge University Press, 2010.

[2] Y. Levin & F. B. Rizzato, *Phys. Rev. E* **74**, 066605 (2006).

[3] A. J. Ward & J. B. Pendry *J. Mod. Opt.* **43**, 773 (1996).

[4] H. Chen, C. T. Chan, & P. Sheng, *Nat. Mater.* **9**, 387 (2010).

[5] J. B. Pendry, D. Schurig & D. R. Smith, *Science* **312**, 1780 (2006).

[6] J. B. Pendry, A. Aubry, D. R. Smith, & S. A. Maier, *Science* **337**, 549 (2012).

[7] Schurig, D. *et al.* *Science* **314**, 977 (2006).

[8] P.-Y. Chen, J. Soric & A. Alu, *Adv. Mater.* **24**, OP281 (2012).

[9] J. B. Pendry, *Phys. Rev. Lett.* **85**, 3966 (2000).

[10] S. Han, Y. Xiong, D. Genov, Z. Liu, G. Bartal, and X. Zhang, *Nano Letters* **4**, 4243 (2008).

[11] D. A. Roberts, M. Rahm, J. B. Pendry, and D. R. Smith, *Appl. Phys. Lett.* **93**, 251111 (2008).

[12] N. Engheta, *Science* **317**, 1698 (2007).

[13] B. Wood & J. B. Pendry, *J. Phys.: Condens. Matter* **19**, 076208 (2007).

[14] F. Magnus *et al.*, *Nat. Mater.* **7**, 295 (2008).

[15] A. Sanchez, C. Navau, J. Prat-Camps, & D.-X. Chen, *New J. Phys.* **13**, 093034 (2011).

[16] S. Narayana & Y. Sato, *Advanced Materials* **24**, 71 (2012).

[17] F. Gomory, M. Solovyov, J. Souc, C. Navau, J. Prat-Camps, and A. Sanchez, *Science* **335**, 1466 (2012).

[18] F. Yang, Z. L. Mei, T. Y. Jin & T. J. Cui, *Phys. Rev. Lett.* **109**, 053902 (2012).

[19] W. X. Jiang, C. Y. Luo, H. F. Ma, Z. L. Mei & T. J. Cui, *Scientific Reports* **2**, 956 (2012).

[20] C. Navau, J. Prat-Camps & A. Sanchez, *Phys. Rev. Lett.* **109**, 263903 (2012).

[21] P. P. Cioffi, *J. Appl. Phys.* **33**, 875 (1962).

[22] J. Stajic, *Science* **339**, 1163 (2013).

[23] J. Wrachtrup & F. Jelezko, *J. Phys.: Condens. Matter* **18**, S807 (2006).

[24] N. Y. Yao *et al.*, *Nat. Commun.* **3**, 800 (2012).

[25] L. Childress, J. M. Taylor, A. S. Sorensen & M. D. Lukin, *Phys. Rev. Lett.* **96**, 070504 (2006) .

[26] T. Gaebel *et al.*, *Nat. Phys.* **2**, 408 (2006).

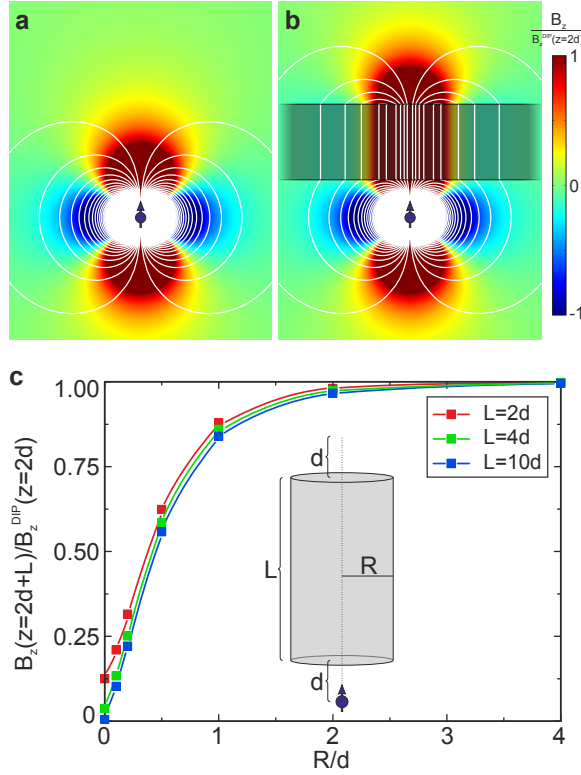


Figure 1: The field of a magnetic source, e.g. a point dipole (a) (field lines in white and vertical field B_z in colors), is exactly transferred an arbitrary distance (b), through an infinite slab of ideal material (shaded region) having $\mu_{\parallel} = \infty$ along the thickness and $\mu_{\perp} = 0$ along the width. (c) When a finite cylindrical piece of radius R of this material is used to transfer the magnetic field of a dipole at a distance d below (inset), the maximum vertical field at a distance d above the ideal hose rapidly tends to the maximum field created by an isolated dipole at a vertical distance $2d$, $B_z^{\text{DIP}}(z = 2d)$, when R increases. When the ideal hose is lengthen, the transferred field slightly decreases and saturates (compare values for $L = 2, 4$ and $10d$).

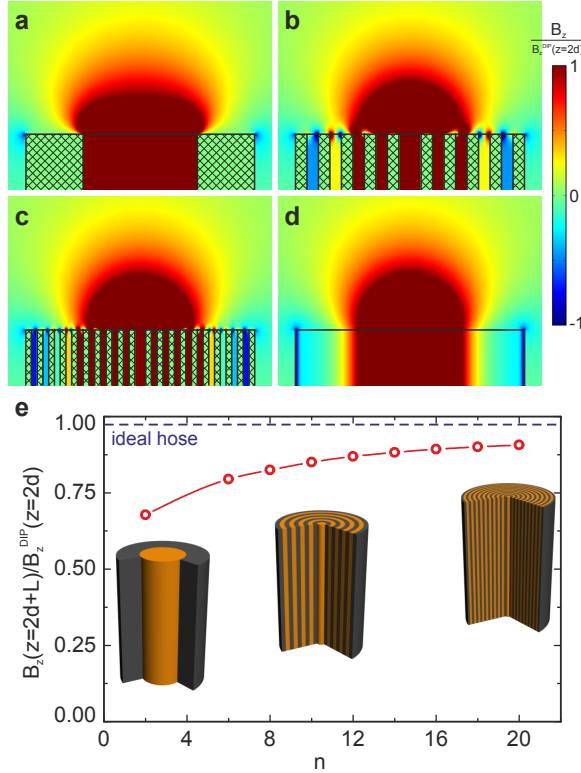


Figure 2: An ideal hose ($\mu_\rho = 0$ and $\mu_z = \infty$), (d), of length $L = 4d$ and radius $R = 2d$ is discretized into (a) $n = 2$, (b) $n = 10$ and (c) $n = 20$ concentric cylindrical shells, half of them SC (shaded) and half FM. Images show the top part of the hoses, where the vertical component of the field transmitted from a dipole placed at a distance d below them is plotted in colors, normalized to $B_z^{\text{DIP}}(z = 2d)$. In (e) the maximum field at a distance d above the discretized hoses (shown in the insets, with SC shells in gray and FM in orange) is plotted as a function of n , showing that they tend to the field transmitted by an ideal hose with the same geometry.

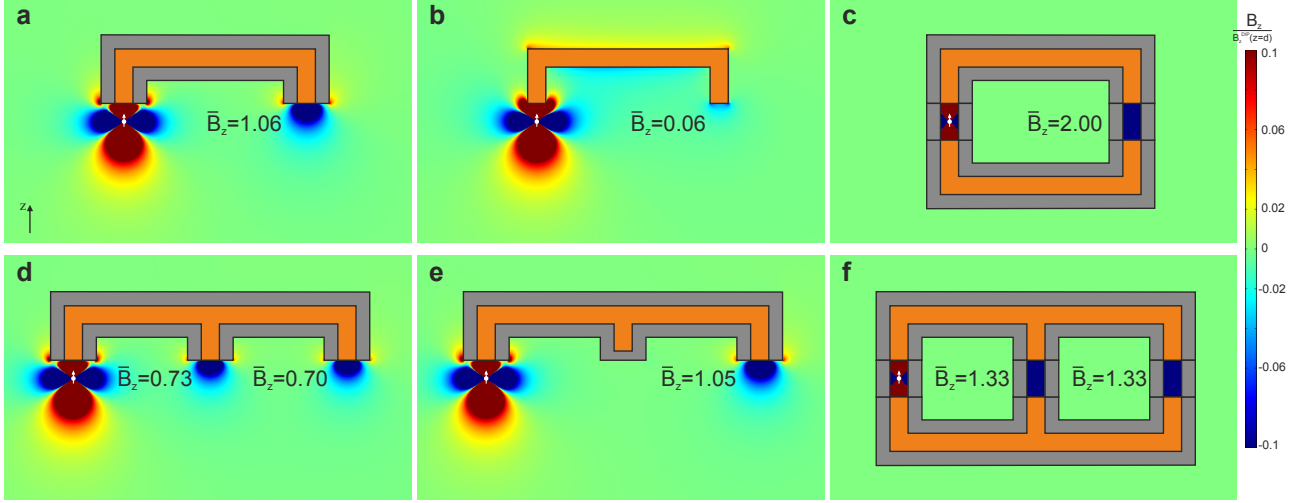


Figure 3: Panels show the vertical field component B_z (in colour scale) in the middle plane of different 3D geometries. The field source is a point dipole (sketched in white) placed at a vertical distance d from the hoses. The FM cylindrical core (orange) has a radius $r = 0.5d$ and the surrounding SC (gray) a thickness $w = 0.75d$. In each simulation it is indicated the average output field \bar{B}_z , calculated as the quotient between the flux that exits each hose end and the area of the ferromagnetic section and normalized to the maximum vertical field created by an isolated dipole at a distance d , $B_z^{\text{DIP}}(z = d)$. Analytical and numerical values of \bar{B}_z fully agree for the closed hoses in (c) and (f). Comparison of (a) and (b) shows the tiny field transmitted when only the FM core is present. Comparison of (a) with (e) shows that increasing the hose length does not significantly decrease the transmitted field. See Supplementary Material Section VII for further discussions of the results.

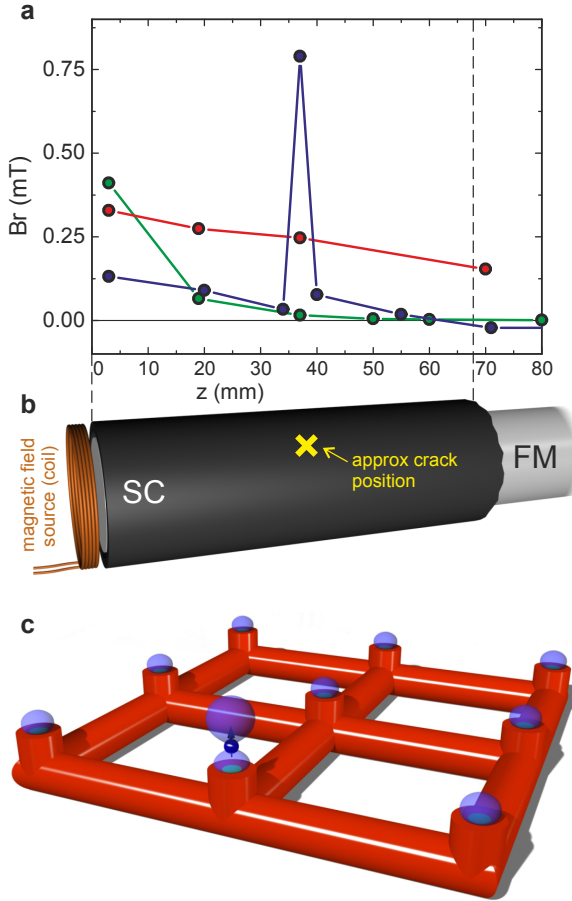


Figure 4: (a) Measurements of radial magnetic field B_r above the SC tube ($r = 23\text{mm}$) at different distances z from the edge of the SC tube [see the sketch (b)]. Green, red and blue curves correspond to the empty, only ferromagnet, and superconductor with ferromagnet cases respectively. Experimental errors on the horizontal and vertical axis are $\Delta z = 2\text{mm}$ and $\Delta B_r = 0.05\text{mT}$ and are omitted for clarity. (c) Artistic illustration on how the field of magnetic sources (e.g. magnetic dipoles) can be routed and used to magnetically connect it to other sources through a hose network. Other tools such as gates interrupting the field transmission at some branches, realized by locally destroying superconductivity (by temperatures above T_C for example), might be also incorporated.

SUPPLEMENTARY MATERIAL

Finite element calculations

All numerical results are obtained by the AC/DC module of Comsol Multiphysics software.

Experimental details

For the experiments we used a high-temperature BiPbSrCaCuO superconducting tube from Can Superconductors and a soft magnetic cylinder made of cobalt-Iron alloy VACOFLUX-17 from Vacuumschmelze. The length of the SC tube was 68mm and that of the FM 140mm. The SC and the FM had similar inner and outer radius (approximately 20mm), respectively, so the FM cylinder could be fit inside the SC tube. The dc current fed in the coil had a value of 3A and the magnetic field on the exterior of the superconducting tube was measured by a Hall probe model HHP-NP from Arepac. All measurements were performed in liquid nitrogen, below the T_C of the SC tube. The whole scan was repeated several times and the high field value at $z \simeq 35\text{mm}$ at the superconductor surface was always systematically obtained.

Table of contents

- I. We present a comparison between the magnetic field transported by a ferromagnetic cylinder and the SC-FM hose.
- II. Transformation optics is applied to design an infinite slab of magnetic material that exactly transfers an initial field distribution to an arbitrary distance.
- III. The field that can be transferred by a finite cylindrical piece of the slab designed in the previous section (named an *ideal hose*) is evaluated depending on its radius and length. We add a demonstration of the fact that even when the ideal hose has a finite radius, there is a part of the magnetic field of the source at one end of the hose that is transferred to the other end independently of the length of the hose.
- IV. The hose is discretized using a number of pieces of homogeneous superconducting and ferromagnetic materials and its transfer capabilities are numerically evaluated as a function of the discretization, remarking the physical correspondences with the ideal hose.
- V. The simplest discretization of the hose consisting on a ferromagnetic cylindrical core surrounded by a superconducting cylinder (*SC-FM hose*) is studied and its performance for magnetic field transfer is evaluated. We obtain some optimized geometrical parameters for an effective field transmission.
- VI. We analytically solve the magnetostatic problem of a magnetic source inside a superconducting tube that has some ferromagnetic pieces embedded in it. In this case, simple analytical formulas for the field transmission are obtained.
- VII. Finally, we numerically analyze the case of closed hoses (finding complete agreement with the analytical results of section VI) and also open hoses. The simulations demonstrate the capabilities of open hoses for connecting magnetic sources and for transmitting their fields.

I. COMPARISON BETWEEN THE MAGNETIC FIELD TRANSMITTED BY A FERROMAGNETIC CYLINDER AND THE SC-FM HOSE

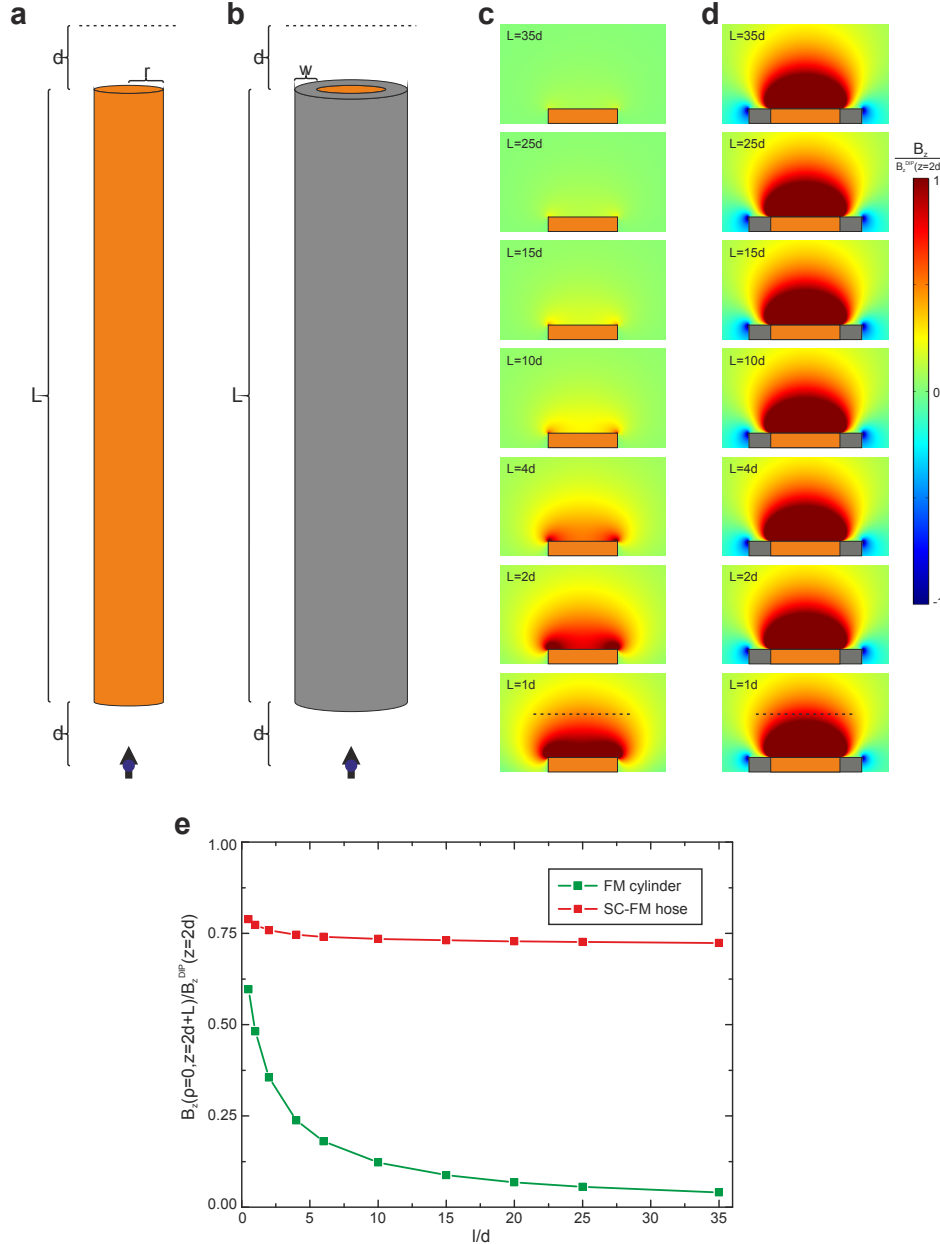


Figure S1: (a) An ideal cylindrical ferromagnetic (FM) material (in orange, with a radius $r = 0.8d$) can transmit the field of a magnetic source (in this case a point dipole, sketched in blue), but the field that reaches the top end of the FM rapidly decays as its length (L) increases because the field leaks through the lateral face and returns to the source. This is clearly shown in the numerical calculations presented in (c), where colors represent the vertical field component B_z at the top of the FM for different L 's, normalized to the maximum vertical field created by an isolated dipole at a distance $2d$, $B_z^{\text{DIP}}(z = 2d)$. (b) In a SC-FM magnetic hose, composed by an ideal superconducting (SC) shell (in gray, with a wall thickness $w = 0.5d$) surrounding a FM core (orange), the field can be transmitted at arbitrary distances, as demonstrated by the numerical calculations presented in (d). In (e) the maximum vertical field at a distance d above the top end surface (always found at $\rho = 0$), $B_z(\rho = 0, z = 2d + L)$, is plotted as a function of the length for the two studied cases, showing that the field above the FM [case (a)] rapidly decays with L , which prevents transporting static magnetic fields at large distances with this strategy. On the contrary, the field transmitted by the SC-FM hose [case (b)] remains highly independent on its length. The relative permeability used in the calculations is $\mu = 10^5$ for the FM and $\mu = 10^{-5}$ for the SC parts.

II. INFINITE SLAB MATERIAL TO EXACTLY TRANSFER THE MAGNETIC FIELD BY TRANSFORMATION OPTICS

A. Material design by transformation optics

Given an initial 3D field distribution $\mathbf{H}(\mathbf{r})$ we want to design a slab material that extends from $z = z_1$ to $z = z_2 > z_1$ and that transfers the field from the semi-infinite region $z > z_1$ to $z > z_2$.

To determine the required material we use *transformation optics* technique [1]. This allows to magnetically characterize the material (i.e. to determine the permeability tensor) needed to transfer the field as desired. We first determine the appropriate space transformation, which is divided in three different parts. If we denote the original empty unaltered space [Fig. S2(a)] by coordinates $\mathbf{r} = (x, y, z)$ and the transformed space by coordinates $\mathbf{r}' = (x', y', z')$ the transformation can be expressed as

$$x' = x, \quad y' = y, \quad z' = z, \quad z \in (-\infty, z_1) \Leftrightarrow z' \in (-\infty, z_1); \quad (\text{S1})$$

$$x' = x, \quad y' = y, \quad z' = \frac{z_2 - z_1}{\xi}(z - z_1) + z_1, \quad z \in [z_1, z_1 + \xi) \Leftrightarrow z' \in [z_1, z_2); \quad (\text{S2})$$

$$x' = x, \quad y' = y, \quad z' = z + (z_2 - z_1 - \xi), \quad z \in [z_1 + \xi, \infty) \Leftrightarrow z' \in [z_2, \infty). \quad (\text{S3})$$

This transformation keeps the lower region $z \in (-\infty, z_1)$ unaltered and vertically shifts the upper region from $z = z_1 + \xi$ to $z' = z_2$ [Fig. S2(b)]. To ensure the continuity of the transformed space the remaining intermediate region $z \in [z_1, z_1 + \xi)$ is linearly expanded between $z' = z_1$ and $z' = z_2$ [Fig. S2(c)]. The desired situation in which all the field above z_1 is shifted to z_2 is achieved in the limit case where $\xi \rightarrow 0$; then the expanded space tends to be null (this ensures a null magnetic energy density inside the material region, which is totally transferred above).

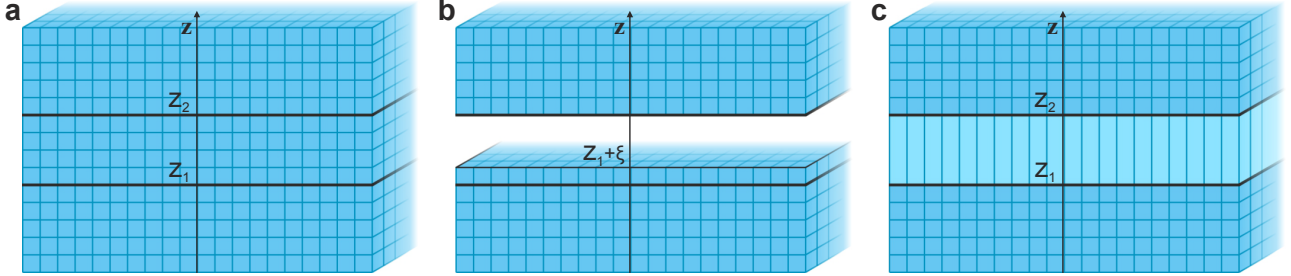


Figure S2: Sketch of the space transformation, which is divided in three parts. Starting from a cartesian unperturbed space (a), the semi infinite space $z > z_1 + \xi$ is shifted to $z > z_2$ (b). (c) Finally, the remaining space between $z = z_1$ and $z = z_1 + \xi$ is expanded leading to a continuous transformed space.

1. Required material

Using the space transformations (S1-S3) we can determine the material that has to be placed in each region by using [1, 2]

$$\mu'(\mathbf{r}') = \frac{\Lambda \cdot \mu(\mathbf{r}) \cdot \Lambda^T}{\det(\Lambda)}, \quad (\text{S4})$$

where $\mu(\mathbf{r})$ is the relative permeability tensor of the original empty untransformed space that is $\mu = \mathbb{1}$ and

$$\Lambda_k^{j'} \equiv \frac{\partial x^{j'}}{\partial x^k}. \quad (\text{S5})$$

Applying it to our case, the matrix Λ and the permeability tensor for each region are

$$\Lambda = \mathbb{1}, \quad \mu = \mathbb{1}, \quad z' \in (-\infty, z_1); \quad (\text{S6})$$

$$\Lambda = \left(1, 1, \frac{z_2 - z_1}{\xi}\right) \cdot \mathbb{1}, \quad \mu = \left(\frac{\xi}{z_2 - z_1}, \frac{\xi}{z_2 - z_1}, \frac{z_2 - z_1}{\xi}\right) \cdot \mathbb{1}, \quad z' \in [z_1, z_2); \quad (\text{S7})$$

$$\Lambda = \mathbb{1}, \quad \mu = \mathbb{1}, \quad z' \in [z_2, \infty). \quad (\text{S8})$$

Note that, even though the upper space is transformed through the transformation of Eq. (S3), this is a space translation that does not require to place any material in the upper region $z' > z_2$ [Eq. (S8)]. This means that it is only necessary to put an homogeneous anisotropic material in the intermediate region between $z' = z_1$ and $z' = z_2$. For the case $\xi \rightarrow 0$ the required material is $\mu_{x'x'} = \mu_{y'y'} \rightarrow 0$ and $\mu_{z'z'} \rightarrow \infty$.

It is worth to remark that all the previous Λ and μ matrices expressed in the cartesian basis have the same form when are expressed in the usual cylindrical basis [then $\mathbf{r} = (\rho, \phi, z)$ and $\mathbf{r}' = (\rho', \phi', z')$ are the coordinates of the initial undeformed and the transformed spaces respectively].

2. Field expressions

From transformation optics theory we can determine the field distribution in the whole transformed space. The field in the transformed space $\mathbf{H}'(\mathbf{r}')$ is found applying [3]

$$\mathbf{H}'(\mathbf{r}') = T(\mathbf{r}') \cdot \mathbf{H}(\mathbf{r}(\mathbf{r}')) , \quad (\text{S9})$$

where $\mathbf{H}(\mathbf{r})$ is the original field distribution before the space transformation and T is the matrix

$$T \equiv \begin{pmatrix} \frac{\partial x}{\partial x'} & \frac{\partial y}{\partial x'} & \frac{\partial z}{\partial x'} \\ \frac{\partial x}{\partial y'} & \frac{\partial y}{\partial y'} & \frac{\partial z}{\partial y'} \\ \frac{\partial x}{\partial z'} & \frac{\partial y}{\partial z'} & \frac{\partial z}{\partial z'} \end{pmatrix} . \quad (\text{S10})$$

Using Eqs. (S1-S3) we find that $T = \mathbb{1}$ for the lower and upper regions $z' \in (-\infty, z_1)$ and $z' \in [z_2, \infty)$ respectively. In the intermediate region

$$T = \left(1, 1, \frac{\xi}{z_2 - z_1} \right) \cdot \mathbb{1}, \quad z' \in [z_1, z_2) \quad (\text{S11})$$

so that we can find the expressions for the magnetic field \mathbf{H}' and the magnetic induction \mathbf{B}' [using Eqs. (S6-S8)] in the whole space for the relevant case $\xi \rightarrow 0$. In the cylindrical basis we find

$$\mathbf{H}'(\rho', \phi', z') = \mathbf{H}(\rho', \phi', z'), \quad \mathbf{B}'(\rho', \phi', z') = \mu_0 \mathbf{H}(\rho', \phi', z'), \quad z' \in (-\infty, z_1) \quad (\text{S12})$$

$$\begin{cases} H'_\rho(\rho', \phi', z') = H_\rho(\rho', \phi', z_1) \\ H'_\phi(\rho', \phi', z') = H_\phi(\rho', \phi', z_1), \\ H'_z(\rho', \phi', z') = 0 \end{cases} \quad \begin{cases} B'_\rho(\rho', \phi', z') = 0 \\ B'_\phi(\rho', \phi', z') = 0, \\ B'_z(\rho', \phi', z') = \mu_0 H_z(\rho', \phi', z_1) \end{cases} \quad z' \in [z_1, z_2) \quad (\text{S13})$$

$$\begin{cases} H'_\rho(\rho', \phi', z') = H_\rho(\rho', \phi', z' - (z_2 - z_1)) \\ H'_\phi(\rho', \phi', z') = H_\phi(\rho', \phi', z' - (z_2 - z_1)), \\ H'_z(\rho', \phi', z') = H_z(\rho', \phi', z' - (z_2 - z_1)) \end{cases} \quad \begin{cases} B'_\rho(\rho', \phi', z') = \mu_0 H_\rho(\rho', \phi', z' - (z_2 - z_1)) \\ B'_\phi(\rho', \phi', z') = \mu_0 H_\phi(\rho', \phi', z' - (z_2 - z_1)), \\ B'_z(\rho', \phi', z') = \mu_0 H_z(\rho', \phi', z' - (z_2 - z_1)) \end{cases} \quad z' \in [z_2, \infty) \quad (\text{S14})$$

From these expression some points are worth to be remarked. First notice that inside the material [Eq. (S13)] magnetic induction \mathbf{B}' is completely vertical and the z component has the same value as the initial distribution at z_1 , independently on z' . The lack of horizontal components of induction field inside the material is ensured by the transformation, which in the limit case $\xi \rightarrow 0$ represents a vertical expansion of an infinitesimal space. On the contrary, magnetic field \mathbf{H}' inside the material is horizontal [Eq. (S13)] and has the value of the original distribution at z_1 , so that it neither depends on z' . As neither \mathbf{H}' nor \mathbf{B}' depend on the vertical coordinate inside the material this ensures that the field can be exactly transferred from z_1 to an arbitrary distance above (as long as ξ is small enough, i.e. $\xi \ll z_2 - z_1$).

It is clearly seen that the energy density $\mathbf{B}' \cdot \mathbf{H}'$ inside the material is zero because induction and magnetic fields are perpendicular. As the magnetic field distribution in the lower region is unaltered [as seen from Eq. (S12), because the space in this region is kept undistorted by the transformation], the magnetic energy density that in the original distribution was between $z = z_1$ and $z = z_2$ is completely transferred to the upper region, $z > z_2$.

Finally the field in the upper part [Eq. (S14)] is exactly the same field distribution that originally was at $z > z_1$, vertically shifted to $z' > z_2$. This confirms the transfer of magnetic field at an arbitrary distance $z_2 - z_1$.

B. Magnetic description of the material through the pole distributions

When a given magnetic field interacts with a passive magnetic material its effect can be totally interpreted as the field created by a certain distribution of volume (ϱ) and surface (σ) magnetic poles, replacing the material by these poles. The general expressions for these pole densities are

$$\varrho = -\nabla \mathbf{M} = \nabla \mathbf{H}, \quad (\text{S15})$$

$$\sigma = -(\mathbf{M}^{OUT} - \mathbf{M}^{IN}) \cdot \hat{n} = (\mathbf{H}^{OUT} - \mathbf{H}^{IN}) \cdot \hat{n}, \quad (\text{S16})$$

where \hat{n} is a unitary vector pointing outwards from the material volume.

Now we can determine the pole distributions from the field expressions found in the previous subsection II A. Using Eqs. (S12-S14), surface pole distributions at the lower and upper material boundaries $\sigma(z' = z_1)$ and $\sigma(z' = z_2)$, as well as volume poles for the case $\xi \rightarrow 0$ are found to be

$$\sigma(z' = z_1) = -H_z(\rho', \phi', z_1), \quad (\text{S17})$$

$$\sigma(z' = z_2) = H_z(\rho', \phi', z_1), \quad (\text{S18})$$

$$\varrho = \frac{1}{\rho'} \frac{\partial}{\partial \rho'} (\rho' H_\rho(\rho', \phi', z_1)) + \frac{1}{\rho'} \frac{\partial}{\partial \phi'} H_\phi(\rho', \phi', z_1). \quad (\text{S19})$$

Notice that poles only depend on the original field distribution at $z = z_1$. Surface poles in the top and the bottom surfaces of the material are exactly the same with opposite signs so that the summation of the surface charge cancels. Volume poles do not depend on z' within the material and the integration of the volume poles along any horizontal plane vanishes so that the total magnetic charge is 0.

For the particular case of a vertical magnetic dipole with magnetic moment m placed at the origin the axial symmetry simplifies these expressions and they become

$$\sigma(z' = z_1) = -\sigma(z' = z_2) = -\frac{m}{4\pi} \left(\frac{3z_1^2}{(\rho'^2 + z_1^2)^{\frac{5}{2}}} - \frac{1}{(\rho'^2 + z_1^2)^{\frac{3}{2}}} \right), \quad (\text{S20})$$

$$\varrho = \frac{m}{4\pi} \left(\frac{-9\rho'^2 z_1 + 6z_1^3}{(\rho'^2 + z_1^2)^{\frac{7}{2}}} \right). \quad (\text{S21})$$

III. FINITE PIECE OF SLAB WITH AXIAL SYMMETRY (IDEAL HOSE)

In this section we evaluate the performance of a cylindrical piece of radius R and length L of the slab described in section II to transfer the field from a source at one end of the material (below in the figure) to a point at the opposite end (above). We assume axial symmetry and the permeability components of the material expressed in the cylindrical basis are set to $\mu_\rho \rightarrow 0$ ($\mu_\phi \rightarrow 0$) and $\mu_z \rightarrow \infty$; we call this an *ideal hose*. Although being a part of the material described in the previous section, the present cylinder extends to a finite radius and does no longer result from a space transformation and, hence, fields and poles cannot be determined from transformation optics theory.

To evaluate its performance we assume a centered vertically-aligned magnetic dipole at a distance d below the bottom end of the material [see Fig. S3(a)]. If the dipole is placed at the origin, following the notation of the previous section, we can identify $d = z_1$ and $L = z_2 - z_1$. From finite-element simulations we calculate the vertical field B_z at a distance d above the top end of the material ($z = 2d + L$) and we plot the maximum value (always found at $\rho = 0$) as a function of R and L (for numerical calculations we use $\mu_\rho = 10^{-5}$ and $\mu_z = 10^5$). Dimensions are normalized to d and field is normalized to the maximum vertical field created by an isolated dipole at a distance $2d$, $B_z^{\text{DIP}}(z = 2d)$.

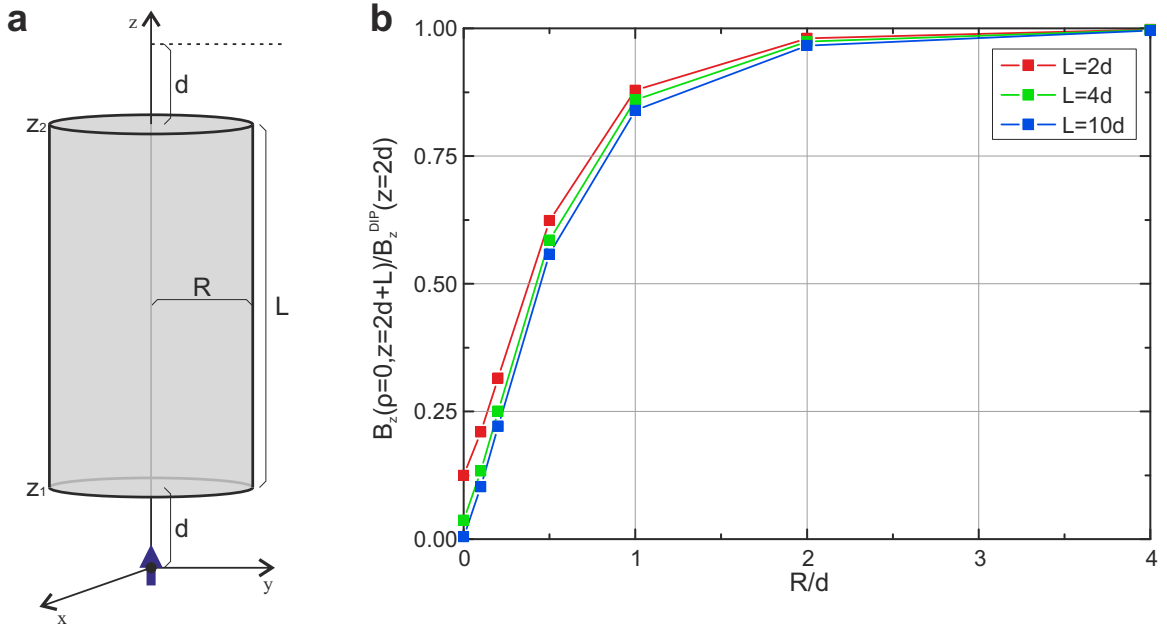


Figure S3: (a) Scheme of the studied geometry. (b) Plots of maximum vertical field normalized to the maximum field created by an isolated dipole at a distance $2d$ as a function of the normalized radius R/d and for different lengths.

Numerical results are shown in Fig. S3(b). We observe that for $R = 4d$ the maximum field is approximately the same as the maximum created by an isolated dipole at a distance $2d$, i.e. the material behaves as if it was an ideal infinite slab (as in section II). This property is approximately maintained even for radii as small as $R = 2d$.

Another interesting property is that the maximum transferred field decreases when the material length increases. However, it rapidly saturates to a certain non-zero value (see the demonstration in the following subsection) that depends on R .

It is worth to notice that the decrease in the transferred field due to increasing L is more evident for small radii; for large radii the material approximates to the infinite slab case where the transferred field does not depend on L .

In the following subsection we will demonstrate that such ideal hose transmits a non-zero field to arbitrarily large distances. Based on Maxwell equations we will also find that

- Surface poles in the bottom and top ends are exactly the same with opposite signs for $\rho < R$ (as demonstrated for the infinite case, section II).
- Volume poles appearing along the material do not depend on the z coordinate for $\rho < R$ (as demonstrated

for the infinite case, section II).

- A certain surface pole distribution appears in the lateral surface $\rho = R$ and it does depend on the z coordinate. The main role of these poles is to guarantee that there is no radial field on the lateral surface, so that no magnetic flux leaks through this surface (totally transferring the field distribution that there is in the bottom end to the top end).

A. Demonstration that a non-zero field is transmitted to an arbitrary distance along an ideal hose with finite radius

We want to demonstrate that a cylindrical piece of material with radius R and length L and relative permeabilities $\mu_\rho \rightarrow 0$ and $\mu_z \rightarrow \infty$ creates a certain non-zero field on the top end when a magnetic field source is placed below the bottom end, independently on L .

We denote the bottom end surface at $z = z_1$ as s_1 , the top end surface at $z = z_2$ as s_2 and the lateral surface $\rho = R$ as s_l and we assume axial symmetry.

Applying magnetostatic boundary conditions and taking into account that there are no free currents we can establish

$$H_\rho^{\text{OUT}}(\rho, z_1) = H_\rho^{\text{IN}}(\rho, z_1), \quad (\text{S22})$$

$$H_z^{\text{OUT}}(\rho, z_1) = \mu_z H_z^{\text{IN}}(\rho, z_1), \quad (\text{S23})$$

$$H_\rho^{\text{OUT}}(\rho, z_2) = H_\rho^{\text{IN}}(\rho, z_2), \quad (\text{S24})$$

$$H_z^{\text{OUT}}(\rho, z_2) = \mu_z H_z^{\text{IN}}(\rho, z_2), \quad (\text{S25})$$

$$H_\rho^{\text{OUT}}(R, z) = \mu_\rho H_\rho^{\text{IN}}(R, z), \quad (\text{S26})$$

$$H_z^{\text{OUT}}(R, z) = H_z^{\text{IN}}(R, z), \quad (\text{S27})$$

where IN and OUT superscripts refer to points inside and outside the material in the interfaces, respectively.

Applying magnetostatic Maxwell equations

$$\nabla \times \mathbf{H} = 0 \quad \Rightarrow \quad \frac{\partial}{\partial z} H_\rho^{\text{IN}}(\rho, z) = \frac{\partial}{\partial \rho} H_z^{\text{IN}}(\rho, z), \quad (\text{S28})$$

$$\nabla \cdot \mathbf{B} = 0 \quad \Rightarrow \quad \frac{\partial}{\partial z} (\mu_z H_z^{\text{IN}}(\rho, z)) = -\frac{1}{\rho} \frac{\partial}{\partial \rho} (\rho \mu_\rho H_\rho^{\text{IN}}(\rho, z)). \quad (\text{S29})$$

The relation between the magnetic field \mathbf{H}^{IN} and the magnetic induction \mathbf{B}^{IN} or the magnetization \mathbf{M}^{IN} inside the material can be established through its permeability. If the material is diagonal then

$$B_\rho^{\text{IN}} = \mu_0 \mu_\rho H_\rho^{\text{IN}}, \quad (\text{S30})$$

$$M_z^{\text{IN}} = (\mu_z - 1) H_z^{\text{IN}}. \quad (\text{S31})$$

If the magnetic field has no singular values then $\mu_\rho \rightarrow 0$ yields $B_\rho^{\text{IN}} = 0$. If the magnetic field has a finite value then the magnetization of the material also has to have a well determined value. This implies that if $\mu_z \rightarrow \infty$ then necessarily $H_z^{\text{IN}} = 0$. For these reasons in all points within the material where the *magnetic field has no singularities* it can be stated that

$$\mu_\rho H_\rho^{\text{IN}} = 0, \quad (\text{S32})$$

$$H_z^{\text{IN}} = 0. \quad (\text{S33})$$

This condition is guaranteed in all the interior points, however boundaries have to be carefully discussed. No singular field values appear within the top and bottom ends except in the circular edges $\rho = R$ where pole densities can be arbitrarily high. Regarding the lateral surface, we only use $H_\rho^{\text{OUT}}(R, z) = 0$, which is enough to ensure that no flux leaks through this surface. This condition is guaranteed if the material is covered by a thin superconducting shell, which does not represent a significant modification of the problem. Due to this, the material can be studied by dividing it into two different regions, $\rho < R$ and $\rho = R$.

In the first one no field singularities are found so that equations (S32) and (S33) hold and we can simplify Eqs. (S28) and (S29) as

$$\frac{\partial}{\partial z} H_\rho^{\text{IN}}(\rho, z) = 0, \quad \rho < R; \quad (\text{S34})$$

$$\frac{\partial}{\partial z} (\mu_z H_z^{\text{IN}}(\rho, z)) = 0, \quad \rho < R; \quad (\text{S35})$$

which allows to combine Eq. (S34) with Eqs. (S22) and (S24), and Eq. (S35) with Eqs. (S23) and (S25), leading to ($z_1 < z < z_2$)

$$H_\rho^{\text{OUT}}(\rho, z_1) = H_\rho^{\text{IN}}(\rho, z_1) = H_\rho^{\text{IN}}(\rho, z) = H_\rho^{\text{IN}}(\rho, z_2) = H_\rho^{\text{OUT}}(\rho, z_2), \quad \rho < R; \quad (\text{S36})$$

$$H_z^{\text{OUT}}(\rho, z_1) = \mu_z H_z^{\text{IN}}(\rho, z_1) = \mu_z H_z^{\text{IN}}(\rho, z) = \mu_z H_z^{\text{IN}}(\rho, z_2) = H_z^{\text{OUT}}(\rho, z_2), \quad \rho < R. \quad (\text{S37})$$

In the second region, corresponding to the lateral surface,

$$H_\rho^{\text{OUT}}(R, z) = 0, \quad \rho = R. \quad (\text{S38})$$

From Eqs. (S36) and (S37) it is demonstrated that the field distribution that there is below the bottom end of the material $\mathbf{H}^{\text{OUT}}(\rho, z_1)$ is exactly transferred above the top end of the material (for $\rho < R$), independently on its length L . In order to demonstrate that some field is transferred from the bottom to the top for an arbitrary L , it only remains to demonstrate that, given a source of magnetic field placed below the material ($z < z_1$), the field below the bottom end of the material is different from zero.

The field at the bottom end of the material is

$$\mathbf{H}^{\text{OUT}}(\rho, z_1) = \mathbf{H}_a^{\text{OUT}}(\rho, z_1) + \mathbf{H}_d^{\text{OUT}}(\rho, z_1), \quad (\text{S39})$$

where $\mathbf{H}_a^{\text{OUT}}(\rho, z_1)$ is the applied field created by the magnetic source and $\mathbf{H}_d^{\text{OUT}}(\rho, z_1)$ is the demagnetizing field created by the magnetic poles appearing in the material below the bottom end surface. There are four different poles in the material: surface poles appearing in the bottom end surface s_1 , surface poles in the top end s_2 , surface poles in the lateral surface s_l and volume poles inside the material.

Surface (σ) and volume (ϱ) poles densities can be calculated through

$$\sigma = -(\mathbf{M}^{\text{OUT}} - \mathbf{M}^{\text{IN}}) \cdot \hat{n} = (\mathbf{H}^{\text{OUT}} - \mathbf{H}^{\text{IN}}) \cdot \hat{n}, \quad (\text{S40})$$

$$\varrho = -\nabla \mathbf{M} = \nabla \mathbf{H}, \quad (\text{S41})$$

where \hat{n} is a unitary vector pointing outwards from the material volume. Applying it to calculate surface poles at s_1 , s_2 and volume poles ($\rho < R$) using Eqs. (S36-S37) and Eqs. (S32-S33) we obtain

$$\sigma_1 = -H_z^{\text{OUT}}(\rho, z_1) + H_z^{\text{IN}}(\rho, z_1) = -H_z^{\text{OUT}}(\rho, z_1), \quad (\text{S42})$$

$$\sigma_2 = H_z^{\text{OUT}}(\rho, z_2) - H_z^{\text{IN}}(\rho, z_2) = H_z^{\text{OUT}}(\rho, z_2) = H_z^{\text{OUT}}(\rho, z_1), \quad (\text{S43})$$

$$\varrho = \frac{1}{\rho} \frac{\partial}{\partial \rho} (\rho H_\rho^{\text{IN}}(\rho, z)) + \frac{\partial}{\partial z} H_z^{\text{IN}}(\rho, z) = \frac{1}{\rho} \frac{\partial}{\partial \rho} (\rho H_\rho^{\text{OUT}}(\rho, z_1)). \quad (\text{S44})$$

Notice that surface poles at s_1 and s_2 are identical with opposite signs and volume poles do not depend on the vertical position inside the material. More important, these three poles distributions only depend on the field below the bottom end of the material.

Surface poles at the lateral surface s_l ($\rho = R$) can be calculated taking into account Eq. (S38) so that

$$\sigma_l = -H_\rho^{\text{IN}}(R, z). \quad (\text{S45})$$

Now suppose that the field below the bottom end is exactly zero [$\mathbf{H}^{\text{OUT}}(\rho, z_1) = 0$ for $\rho < R$]. Then from equations (S42-S44) there are no surface poles at s_1 and s_2 , nor volume poles. This means there can only be surface poles at s_l (i.e. the demagnetizing field \mathbf{H}_d is the field created only by these surface poles), whose value is determined by the applied field from the source and the demagnetizing field created by themselves [Eq. (S45)]. In general, however, the demagnetizing field that these poles create below the bottom end surface of the material $\mathbf{H}_d^{\text{OUT}}(\rho, z_1)$ will not cancel the applied field created by the source there $\mathbf{H}_a^{\text{OUT}}(\rho, z_1)$, so that $\mathbf{H}^{\text{OUT}}(\rho, z_1) \neq 0$ for some points $\rho < R$, facing a contradiction. This means that, in general, the field below the bottom end surface $\mathbf{H}^{\text{OUT}}(\rho, z_1)$ will not be zero and hence, a certain field will be transferred to the top end surface, independently on L [Eqs. (S36) and (S37)].

IV. DISCRETIZATION OF THE IDEAL HOSE USING SC AND FM CONCENTRIC CYLINDERS

The material described in the previous sections requires $\mu_z \rightarrow \infty$ and $\mu_\rho \rightarrow 0$ and actual materials with such extreme anisotropy do not exist. However an approximation consisting of a series of n alternated ideal superconducting (SC, with $\mathbf{B} = 0$) and ideal soft ferromagnetic (FM, with $\mathbf{H} = 0$) concentric cylinders constitutes a natural discretization of the required material as the ferromagnetic parts provide a large permeability in the z direction and the alternated superconductors prevent the appearance of radial \mathbf{B} field components leading to an effective zero radial permeability.

In a (finite) ideal hose there are surface poles in the top and bottom ends, surface poles in the lateral surface and volume poles within the material. When the material is discretized as explained, inside the superconducting and the ferromagnetic cylinders no volume poles appear because materials are homogeneous, isotropic and linear. However, surface poles appear in the interfaces between the lateral faces of adjacent cylinders. These poles play an equivalent role to the volume poles appearing in the ideal hose. Actually, fixed the radius R , when n increases the distance between consecutive interfaces is reduced and these surface poles resemble the volume poles of the ideal hose.

The surface poles on the top and bottom ends of the ideal hose now appear mainly on the ferromagnetic cylinders' horizontal top and bottom faces ($H_z^{\text{IN}} = 0$ but $H_z^{\text{OUT}} \neq 0$). On the contrary, out of the horizontal faces of the superconducting cylinders $H_z^{\text{OUT}} = 0$ and it can be shown that the magnetic field \mathbf{H} inside them has mainly radial direction so that few surface poles appear in these faces of the superconductors.

Finally, if the most external cylinder is superconducting (the most appropriate choice to prevent field leakage), surface poles appear on the exterior surface (because despite $H_\rho^{\text{OUT}} = 0$, $H_\rho^{\text{IN}} \neq 0$) similarly to that appeared in the lateral surface of the ideal hose.

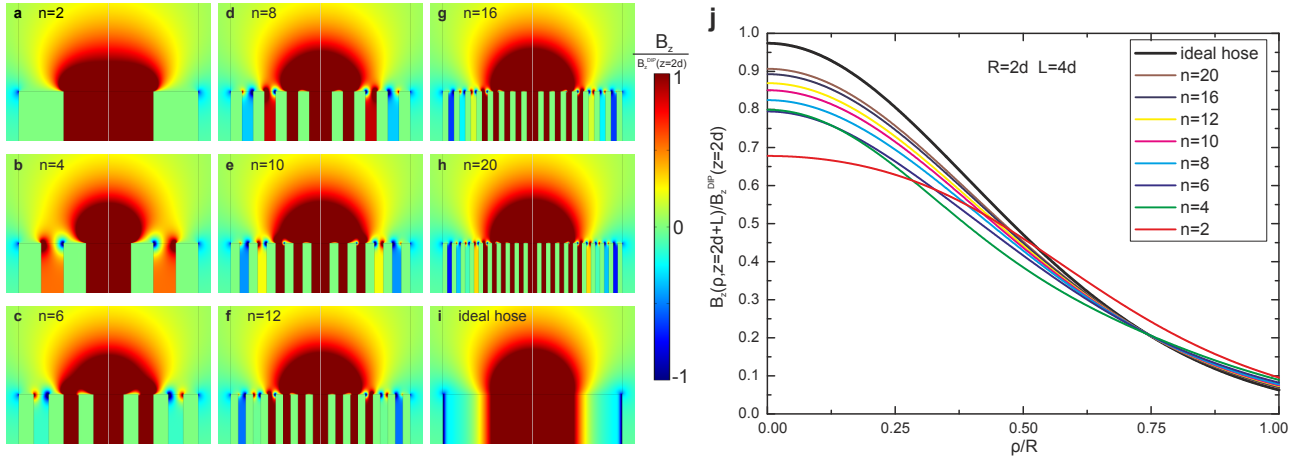


Figure S4: (a-h) Simulation results showing the B_z field component above the top end of hoses with different discretizations compared with the ideal case (i) when a centered dipole is placed below the bottom end. In (j) we present plots of this component along an horizontal line at a distance d above the top end of the hose $B_z(\rho, z = 2d + L)$, normalized to the maximum field of an isolated dipole at a vertical distance $2d$, $B_z^{\text{DIP}}(z = 2d)$. Geometrical parameters used in the simulations are $R = 2d$ and $l = 4d$.

To evaluate the performance of these discretized designs we carried out finite-element simulations of a hose discretized into different number of cylinders when a centered dipolar source is placed at a distance d below it (for numerical calculations we use a relative permeability for the SC cylinders of $\mu^{\text{SC}} = 10^{-5}$ and for the FM ones $\mu^{\text{FM}} = 10^5$). We compare the field above the top end with that appeared in the case of an ideal hose. Results presented in Fig. S4 show that when the number of layers is increased the field at the top tends to the field transmitted by an ideal hose, confirming the presented discretization arguments.

V. SIMPLEST CASE OF A FM CENTRAL CORE SURROUNDED BY A CYLINDRICAL SC SHELL (SC-FM HOSE)

The simplest discretization of an ideal hose is a cylindrical ideal ferromagnetic core (with radius r) surrounded by an ideal superconducting cylinder [with inner radius r and wall thickness w , see Fig. S5(a)]. The SC prevents the flux leakage through the lateral faces, allowing to transfer the field along the *SC-FM hose*.

The main aim of this section is to evaluate the possibility of transmitting the magnetic field from a source placed on one end of a SC-FM hose to the other end. We perform finite-element simulations placing a centered and vertically aligned dipole at a distance d below the bottom end of the hose and we determine the maximum field at a distance d above the top end. In all the studied cases, exploring the field at a distance d above the top end, the maximum value of B_z is always found at the center $\rho = 0$. Nevertheless, at smaller heights closer to the top end surface, field maxima are not found at the center but at $\rho \approx r$, i.e. above the interface between the FM and the SC.

Simulations results are presented in Fig. S5(b) and (c), where the maximum vertical field at a distance d above the top end surface $B_z(\rho = 0, z = 2d + L)$ is presented for a fixed d as a function of r for different values of $R = r + w$ (b) and also for different lengths L (c). Field values are normalized to the maximum vertical field created by an isolated dipole at a vertical distance $2d$, $B_z^{\text{DIP}}(z = 2d)$.

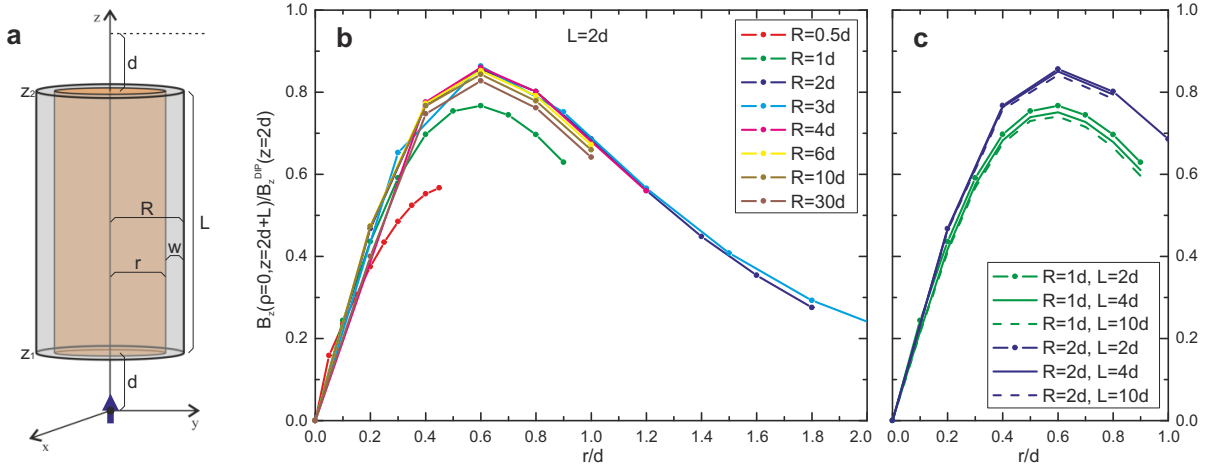


Figure S5: (a) Scheme of the studied geometry, where the ferromagnetic material is represented in orange and the superconducting in gray. (b-c) Plots of the maximum vertical field at a distance d above the top end surface (always found at $\rho = 0$), as a function of the ferromagnetic core radius r and for different R and L .

From these plots some conclusions can be extracted. For small values of $R = r + w$ [red line in Fig. S5(b)] the maximum field continuously increases when increasing r because more field lines are allowed to go into the FM. For larger R , B_z have a maximum at $r \approx 0.6d$; for $r < 0.6d$ some field lines cannot enter in the FM and for $r > 0.6d$ lines enter in the FM but they have room to turn around, going out through the bottom end of the FM and resulting in a lower field on the top. Therefore there is an optimum value of r/d , which depends on the particular field profile given by the magnetic source.

Notice that, although the maximum of each curve is always found at $r \approx 0.6d$ the absolute maximum is not found until $R \approx 2d$. This reveals an important role of the SC, whose field expulsion effect at the bottom end horizontal face allows that some more lines go into the FM. However if we keep increasing R , B_z values slowly tend to decrease. This is because some field lines on the top of the hose cannot return by the exterior of the hose due to its large radius R , (then they should return through the central ferromagnetic core) which results in a lower field on the top of the hose.

Finally, we show in Fig. S5(c) how these results barely change with L , showing a clear saturation effect. This can be understood taking into account that when L is large and is increased a certain ΔL , the extra poles appearing in the top part of the hose have a small effect at the bottom part of the hose, so that the field distribution at the bottom is almost unaffected (and the fraction of field lines that turn around inside the FM and the rest that follow to the top do not practically change).

To sum up, for an upright magnetic dipole at a distance d below the hose, there is an optimum value around $r = 0.6d$ and $w = 1.4d$ ($R = 2d$) for which the field at a distance d above the top end surface is maximum, independently on L .

VI. ANALYTICAL DERIVATION OF PROPERTIES OF SC-FM HOSES

Consider an infinite ideal superconducting tube of inner radius R , infinitely long in the z direction and a magnetic point dipole located in its axis and with magnetic moment $\mathbf{m} = m\hat{z}$. Symmetrically (vertically) with respect the position of the dipole and encased in the superconducting tube, consider two ideally soft ferromagnets of lengths $2S$ located at distance l_s from the dipole. In this section we will analytically find the magnetic field in the different air regions (in the region occupied by the dipole and beyond the ferromagnets) [shown in Fig. S6(d)].

To address this problem we will use the magnetostatic scalar potential. Since there are no free currents, the magnetic field \mathbf{H} in all regions can be obtained from a scalar potential ϕ through $\mathbf{H} = -\nabla\phi$. All the materials involved are considered to be linear, homogeneous and isotropic, so that this scalar potential must satisfy Laplace equation in all regions together with the corresponding boundary conditions.

To solve the problem, we will proceed in several steps. First, we will review different expressions for the scalar potential generated by a single point dipole [Fig. S6(a)]. Second, we will locate this dipole inside a long superconducting tube [Fig. S6(b)] and we will find the new potential. Third, we will add semi-infinite ferromagnets encased inside the superconducting tube [Fig. S6(c)]. Finally, we shall solve the original problem, by considering finite encased ferromagnets [Fig. S6(d)].

For this case we will find the scalar potential in all regions and we will present the corresponding magnetic field expressions, showing that there are configurations for which the field created by the dipole can be transferred to other empty regions beyond the ferromagnets. These regions can be placed as far as desired from the source. Moreover, the value of the transferred field can be very large.

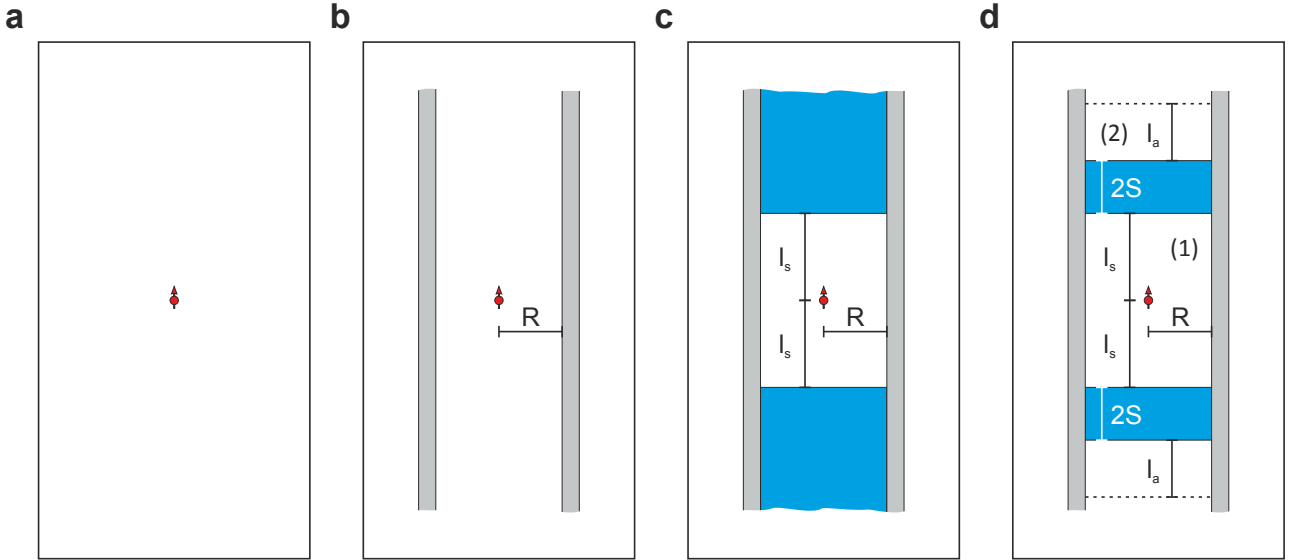


Figure S6: Sketch of the different solved configurations. Figures represent cylinders with the origin on the point dipole position (in red) and z axis coaxial with the cylinders. Gray regions represent ideal superconductor and blue ideally soft ferromagnets.

A. A point magnetic dipole

Consider a point magnetic dipole with magnetic moment $\mathbf{m} = m\hat{z}$, located at the origin of coordinates [Fig. S6(a)]. The scalar magnetic potential $\phi_{dp}(\rho, z)$ (we use standard cylindrical coordinates) can be written as

$$\phi_{dp}(\rho, z) = \frac{m}{4\pi} \frac{z}{(z^2 + \rho^2)^{3/2}} \quad (S46)$$

$$= \frac{m}{4\pi} \int_0^\infty k J_0(k\rho) e^{-k|z|} dk \quad (S47)$$

$$= \frac{m}{4\pi} \frac{2}{\pi} \int_0^\infty k K_0(k\rho) \sin(kz) dk, \quad (S48)$$

where $J_i()$ [$K_i()$] is the Bessel (modified Bessel) function of the first (second) kind of order i .

The vertical component of the magnetic field $H_z(\rho, z) = -\partial\phi_{\text{dp}}(\rho, z)/\partial z$ has zero value at a circular conical surface with the vertex on the origin and defined by $z = \pm\rho/\sqrt{2}$.

B. A point magnetic dipole inside a cylindrical superconducting tube

Consider now that the point dipole is located on the axis of an infinitely long (along z -axis) superconducting tube of interior radius R [Fig. S6(b)]. We shall consider the superconductor (SC) to be ideal so that the magnetic induction field in its interior is $\mathbf{B} = 0$. Implicit in this assumption is that the London penetration depth λ of the SC is much lower than any other dimension involved in the problem. Since the the magnetic field source (the dipole) is in the interior of the tube, the outer radius of the superconducting tube plays no role.

Inside the tube, the general form for the solutions of the Laplace equation, after taking into account the symmetry of the problem, can be written as

$$\begin{aligned}\phi_{\text{tu}}(\rho, z) = & \frac{m}{4\pi} \frac{z}{(z^2 + \rho^2)^{3/2}} \\ & + \int_0^\infty A(k) I_0(k\rho) \sin(kz) dk \\ & + Gz + F,\end{aligned}\quad (\text{S49})$$

where $I_i(x)$ is the modified Bessel function of first kind and order i . $A(k)$ is a function that should be found by considering the boundary conditions. The first term in Eq. S49 is the scalar potential of the dipole, the second term is the contribution of the currents induced in the superconductor [4], and the last two (linear and constant) terms represent a uniform field along z . Choosing $\phi_{\text{tu}} = 0$ at $z = 0$ we have $F = 0$. The boundary condition at $\rho = R$ states that the normal component of the magnetic field must be zero there, because of the superconducting inner surface. Imposing this condition we get

$$A(k) = \frac{m}{2\pi^2} k \frac{K_1(kR)}{I_1(kR)}. \quad (\text{S50})$$

For the linear term, we set $G = 0$, since at large vertical distances the field cannot be different from zero (the rest of terms of ϕ_{tu} vanish when $z \rightarrow \infty$).

Finally, the scalar potential is

$$\begin{aligned}\phi_{\text{tu}}(\rho, z) = & \frac{m}{4\pi} \frac{z}{(z^2 + \rho^2)^{3/2}} \\ & + \frac{m}{2\pi^2} \int_0^\infty k \frac{K_1(kR)}{I_1(kR)} I_0(k\rho) \sin(kz) dk.\end{aligned}\quad (\text{S51})$$

It can be shown [4] that for large $|z|$ both components (modulus) of the magnetic field, for a given ρ , decay exponentially with $|z|$ with a characteristic length of $R/\xi_1 \simeq 0.261R$, being ξ_i the i th root of $J_1(x)$. When $|z| \rightarrow \infty$, the potential tends to $\pm m/(2\pi R^2)$.

C. A point magnetic dipole inside a cylindrical superconducting tube with encased semi-infinite soft ferromagnetic material

Consider now that two semi-infite soft ferromagnetic (FM) materials are encased inside the tube symmetrically with respect the dipole [see Fig. S6(c)], with their tap end surfaces located at $z = \pm l_s$. We assume that the FMs are ideally soft magnetic materials such that their susceptibility is infinite and thus, the magnetic field inside them is zero, $\mathbf{H} = 0$.

Within this assumption, the FMs are equipotential volumes and their effect is to provide a surface at fixed z in which the scalar potential must be constant.

The contribution from the FMs surfaces to the total scalar potential, $\phi_{\text{fm}}(\rho, z)$, implies new boundary conditions at $|z| = l_s$, without modifying the boundary conditions at $\rho = R$. A complete set of solutions that has the proper symmetry can be written as

$$\begin{aligned}
\phi_{\text{te}}(\rho, z) = & \frac{m}{4\pi} \frac{2}{\pi} \int_0^\infty k K_0(k\rho) \sin(kz) dk \\
& + \int_0^\infty A(k) I_0(k\rho) \sin(kz) dk \\
& + \sum_{n=1}^\infty C_n J_0(k_n \rho) \sinh(k_n z) \\
& + Dz + F.
\end{aligned} \tag{S52}$$

where $A(k)$, C_n , k_n , D , and F have to be determined. Note explicitly the two final terms. They represent a uniform field (linear potential) that satisfies the Laplace equation with constant potential at a given z . By choosing $\phi_{\text{te}} = 0$ at $z = 0$, we get $F = 0$.

The boundary condition at $\rho = R$ [i.e. the normal (radial) component of \mathbf{B} must be continuous] is satisfied by considering that the $k_n R$ values are the roots of the $J_1(x)$ function [since $J'_0(x) = -J_1(x)$], $k_n = \xi_n/R$, and that function $A(k)$ is the same as in Eq. S50.

The boundary condition at $|z| = l_s$ leads to

$$C_n = \frac{m}{4\pi} \frac{2e^{-\xi_n l_s / R}}{R^2 \sinh(\xi_n l_s / R) J_0(\xi_n) J_2(\xi_n)}. \tag{S53}$$

The values of C_n can be found after multiplying the equation that emerges from the boundary condition by $P_1(\alpha\rho/R)$ (for arbitrary α), integrating from 0 to R , and using the orthogonality properties of Bessel functions.

The remaining constant D is found by considering the ferromagnets. Indeed, since they are passive elements, the induced magnetic charge on each of them must be zero. To evaluate this charge, we use that the discontinuity of the normal component of the magnetic field at $z = l_s$ is determined by the magnetic pole density induced in this surface (we shall make the treatment at positive z 's; equivalent solutions would be found for $z = -l_s$ due to the symmetry of the problem). Since inside the ferromagnet $\mathbf{H} = 0$, the pole density is

$$\begin{aligned}
\sigma(\rho) = & -H_z(\rho, z = l_s) = \left[\frac{\partial \phi_{\text{te}}(\rho, z)}{\partial z} \right]_{z=l_s} \\
= & \frac{-2l_s^2 + \rho^2}{(l_s^2 + \rho^2)^{5/2}} \\
& + \int_0^\infty \frac{2k^2}{\pi} \frac{K_1(kR)}{I_1(kR)} I_0(k\rho) \cos(kl_s) dk + \\
& + \sum_{n=1}^\infty C_n \frac{\xi_n}{R} J_0(k_n \rho) \cosh(k_n l_s) \\
& + D.
\end{aligned} \tag{S54}$$

It is important to notice that the pole density at the lateral ($\rho = R$) surfaces of the ferromagnet is zero. This is so because in the interface between SC and FM both \mathbf{B} and \mathbf{H} are zero. The total magnetic charge, Q_m , can be now evaluated by integrating the pole density over the $z = l_s$ FM-air interface

$$Q_m = \int_0^R \sigma(\rho) 2\pi \rho d\rho = D\pi R^2. \tag{S55}$$

The first two terms in the previous integral cancel each other (as can be seen by direct integration). The third term equals zero since $\int_0^R \rho J_0(\xi_n \rho / R) d\rho = (R/k) J_1(\xi_n) = 0$. Eq. S55 indicates that $D = 0$, since no net charge can be present in the ferromagnet.

So, finally, the scalar potential is

$$\begin{aligned}
\phi_{\text{te}}(\rho, z) = & \frac{m}{4\pi} \frac{2}{\pi} \int_0^\infty k K_0(k\rho) \sin(kz) dk \\
& + \int_0^\infty \frac{m}{2\pi^2} k \frac{K_1(kR)}{I_1(kR)} I_0(k\rho) \sin(kz) dk \\
& + \sum_{n=1}^\infty \frac{m}{4\pi} \frac{2e^{-\xi_n l_s / R}}{R^2 \sinh(\xi_n l_s / R) J_0(\xi_n) J_2(\xi_n)} J_0(\xi_n \rho / R) \sinh(\xi_n z / R).
\end{aligned} \tag{S56}$$

When $z = l_s$, we have

$$\begin{aligned}\phi_{\text{te}}(z = l_s) &= \frac{m}{4\pi} \frac{1}{l_s^2} \\ &+ \int_0^\infty \frac{m}{2\pi^2} k \frac{K_1(kR)}{I_1(kR)} \sin(kl_s) dk \\ &+ \sum_{n=1}^{\infty} \frac{m}{4\pi} \frac{2e^{-\xi_n l_s / R}}{R^2 J_0(\xi_n) J_2(\xi_n)}.\end{aligned}\quad (\text{S57})$$

We define this quantity as η , $\eta \equiv \phi_{\text{te}}(z = l_s)$. We see that η/η_∞ [defining $\eta_\infty = m/(2\pi R^2)$] only depends on l_s/R . With the values for which we can numerically evaluate η with enough accuracy ($l_s/R \gtrsim 0.1$), we have found that $\eta/\eta_\infty = 1$, so hereafter we will assume this value.

D. A point magnetic dipole inside a cylindrical superconducting tube with encased finite soft ferromagnetic material

We are now ready to find the complete solution for the original problem stated at the beginning of this section. This is, to calculate the magnetic fields in the air gaps of a magnetic hose.

We refer to the Fig. S6(d) and name $\phi_i(\rho, z)$ the scalar potential in region i of the figure. The general solutions that satisfy Laplace equation and the corresponding boundary conditions are of the type (we work in regions 1 and 2, the lower region can be similarly treated as 2 due to the symmetry)

$$\phi_1(\rho, z) = \phi_{\text{te}}(\rho, z) + Mz + N \quad (\text{S58})$$

$$\phi_2(\rho, z) = Pz + Q \quad (\text{S59})$$

Choosing scalar potential zero at $z = 0$, we have $N = 0$. We should now find M, P, Q .

Notice that in the previous subsection the linear term in the potential was zero because the total charge at the surface of the FM must be zero. Now we have two surfaces (tap ends) for each FM, and the total charge in each FM must be zero. Again, we use the fact that in the lateral surface of the FM ($\rho = R$, interface with the SC) the pole density is zero.

Following the arguments and calculations used to evaluate Eq. S55, we find that

$$M = P. \quad (\text{S60})$$

From the continuity of the potential (and taking into account that the FMs are equipotential volumes) we get

$$\eta + Ml_s = P(l_s + 2S) + Q. \quad (\text{S61})$$

We need a third condition. This condition should come from the physical way in which the ends of the hose are connected. If the hose is straight and tends to be infinitely long (we could think in the limiting case of an open hose whose total length is increased up to infinite) there cannot be a uniform field up to infinity and this implies that $P = 0$. From this, $M = 0$ and $Q = \eta$.

However, there is a more interesting configuration. Imagine that in the region 2 after an air gap of length l_a (along z) we connect the two tap ends of the hose, generating a closed tube with two air-gaps: one containing the dipole and of length $2l_s$ and the other containing no magnetic sources and of length $2l_a$ (see Fig. S7). The potential at $z = l_s + 2S + l_a$ must be zero because of the antisymmetry of the solution (or, in other words, since the potential must be continuous, the antisymmetry of the problem assures that it is zero at the 'connexion' plane). We are assuming that the radius of curvature of the closed tube is much larger than R (and the z coordinate refers to positions along the tube). We have then

$$P(l_s + 2S + l_a) + Q = 0. \quad (\text{S62})$$

Eqs. (S60)-(S62) can now be easily solved for M, P , and Q . The final potential functions at regions 1 and 2 are

$$\phi_1(\rho, z) = \phi_{\text{te}}(\rho, z) - \frac{\eta}{l_s + l_a} z, \quad (\text{S63})$$

$$\phi_2(\rho, z) = \eta - \frac{\eta}{l_s + l_a} (z - 2S), \quad (\text{S64})$$

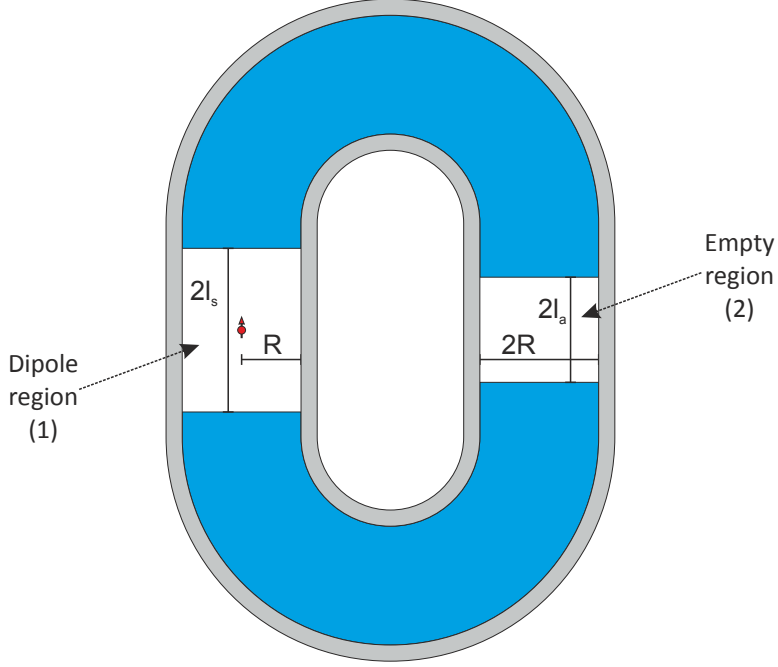


Figure S7: Sketch of a closed magnetic hose. A superconducting tube (gray) is filled by ferromagnetic material (blue) leaving some air spaces, in which we could locate a point dipole (in red).

where η is a function of R and l_s given in Eq. S57 and $\phi_{te}(\rho, z)$ is given in Eq. (S56).

Properties of the closed magnetic hose

From the previous results we can now easily calculate the magnetic fields at any region inside the closed hose. Of special interest is the field in the empty region (region 2). From Eq. S64, the magnetic field in region 2 is uniform and has only z component given by

$$H_z = \frac{\eta}{l_s + l_a}. \quad (\text{S65})$$

This means that the field can be *transferred* to an arbitrary distance from the source, since its magnitude does not depend on S , the (semi)length of the ferromagnetic element.

According to Eq. S65, the magnitude of the field in region 2 can be greatly increased by reducing the l_s gap (keeping the rest of parameters fixed). In particular, and considering $\eta = (m/2\pi R^2)$, the magnitude of the field is inversely proportional to the total air-gaps length $2(l_s + l_a)$. Also, for a fixed l_s , when l_a decreases the magnetic field magnitude in the gap 2 increases. Note also that the field in the dipole region (region 1) is changed by the presence of the region 2. Its effect is an extra uniform field that must be added to the field coming from $\phi_{te}(\rho, z)$.

From the energetic point of view, part of the energy of the dipole field is transferred through the ferromagnet (inside which the energy density is zero since $\mathbf{H} = 0$) up to the empty air region. The amount of energy 'transferred' by the ferromagnet depends on the dimensions of both the dipole-gap and the empty-gap. In general, the smaller l_s is the more energy can be collected and transferred to the air gap. The larger the l_a is the more diluted the energy over the empty air gap is.

Since the length of the FMs plays no role, we could envisage a closed hose with straight air gaps but with any shape (even with small radius of curvature) for the FM part of the hose. In this way we could relax the condition of large curvature radius when 'connecting' the tap ends of the hose (see Fig. S7). Moreover, since the field created by the dipole does not leak outside the hose (due to the superconducting tube) there would be no interaction between the air-gaps through the air outside the hose.

Several air-gaps along a hose could be also envisaged. Locating several dipoles on several air-gaps could be used as a complex system of magnetic dipoles with large interaction at large distance between them.

VII. SC-FM HOSE WITH COMPLEX GEOMETRIES

In this section we numerically study the magnetic field that can be transmitted with a SC-FM hose when it has a more complex geometry than the vertical straight one (studied in section V). In this case we consider a vertical magnetic dipole placed at a distance d of a SC-FM hose whose interior FM core has a radius $r = 0.5d$ and is surrounded by a ideal SC cylinder with inner radius r and wall thickness $w = 0.75d$. The geometrical parameters r and w have been chosen similar to the optimized values found in section V.

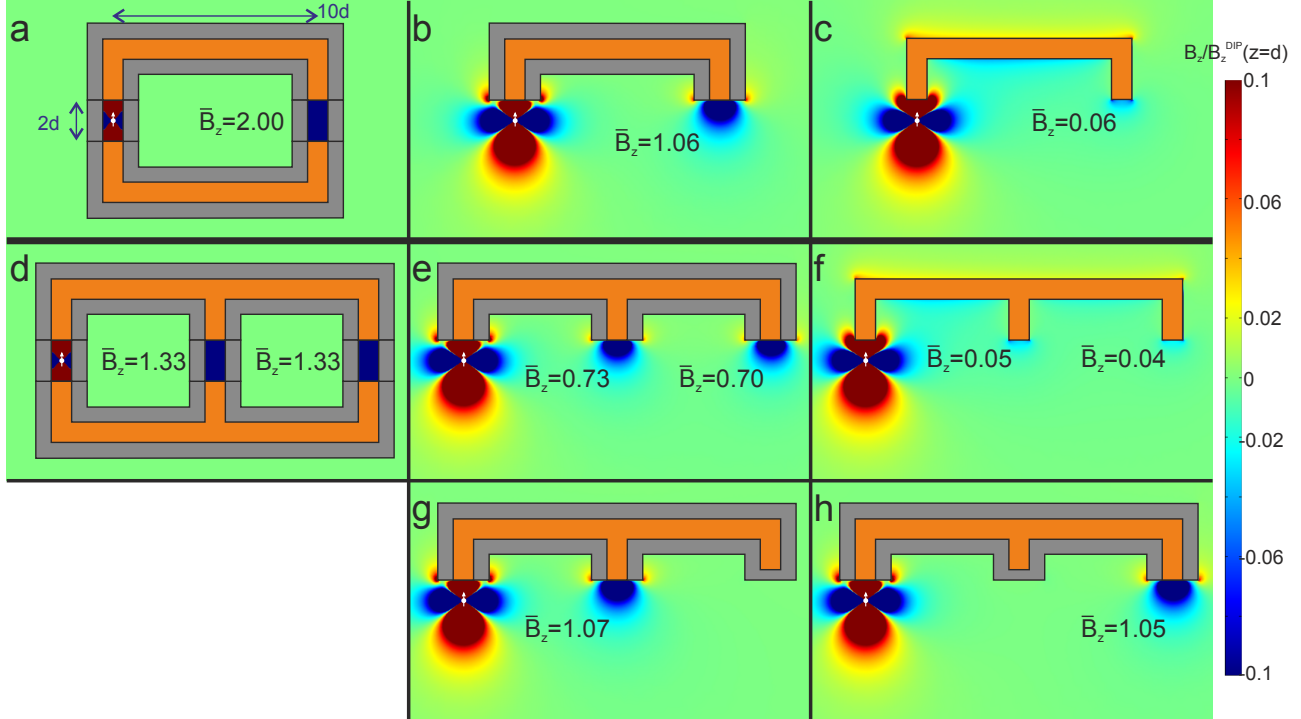


Figure S8: Plots of the vertical field component from 3D finite-element simulations of a curved hose (b) and ramified hoses (e),(g),(h) (FM cores represented in orange and surrounding SC shells in gray). Simulations of the corresponding closed geometries are shown in (a) and (d). For comparison, simulations in which there is only the interior FM core are shown in (c) and (f). In colors we present the calculated vertical field component B_z normalized to the maximum vertical field created by an isolated dipole at a distance d , $B_z^{\text{DIP}}(z = d)$. Numbers indicate the *average output field* (\bar{B}_z), being the average field that gets out of each ferromagnetic surface normalized to $B_z^{\text{DIP}}(z = d)$.

Results for two open geometries are shown in Fig. S8(b) and (e). The first corresponds to a curved hose and the second to a hose that is ramified in two branches. To deduce some properties of the curved and the ramified hose we also present the corresponding closed geometries (a) and (d) which can be analytically solved from the results of section VI. For comparison we also present the cases in which there is only the interior ferromagnetic core. In all the simulations we present the *average output field* \bar{B}_z calculated as the quotient between the flux that exits each hose end and the area of the ferromagnetic section and normalized to the maximum vertical field created by an isolated dipole at a distance d , $B_z^{\text{DIP}}(z = d)$

Closed cases (a) and (d) can be solved through the results of section VI, where we demonstrated that the uniform field inside the empty gap of a non-ramified closed geometry is given by Eq. (S65)

$$B_z = \frac{\mu_0 m}{2\pi R^2} \frac{1}{l_s + l_a}, \quad (\text{S66})$$

where m is the magnetic moment of the dipole and R , l_s and l_a are the geometrical parameters defined in Fig. S7. We consider that $l_s = d$ and $R = r$ and taking into account that the maximum vertical field created by an isolated dipole at distance d is

$$B_z^{\text{DIP}}(z = d) = \frac{\mu_0 2m}{4\pi d^3}, \quad (\text{S67})$$

we find that the average output field in the gap of height $2l_a$ is

$$\bar{B}_z \equiv \frac{B_z}{B_z^{\text{DIP}}(z = d)} = \frac{d^3}{r^2(d + l_a)}. \quad (\text{S68})$$

In case (a) $l_a = d$, and taking into account the geometrical parameters we find that $\bar{B}_z = 2$, in agreement with the simulation.

For the ramified case (d) one can calculate the effective gap equivalent to the two parallel gaps. Since in this case the system behaves as an ideal magnetic circuit the effective gap l_a^{eff} can be calculated through the parallel association formula

$$l_a^{\text{eff}} = \left(\frac{1}{l_{a,1}} + \frac{1}{l_{a,2}} \right)^{-1}. \quad (\text{S69})$$

In this case $l_{a,1} = l_{a,2} = d$, so that $l_a^{\text{eff}} = d/2$. Applying Eq. (S68) and taking into account that the calculated field is equally divided into the two branches we find that the field inside each gap of the ramified hose (d) is $\bar{B}_z = 4/3$, in agreement with the simulations.

Comparing the two closed geometries (a) and (d) one can see that the field in the gap is lower when the hose is ramified. However, in this case, the total average output field (adding up that of the two branches) is larger, because the effective gap becomes smaller when branches are in parallel.

Concerning the open geometries, some conclusions can be outlined:

1. A hose made of an interior FM core surrounded by a SC layer can transmit the field of a point source (e.g. a magnetic dipole) to a given distant point increasing the transmitted field by a large factor (~ 17 in these simulations) respect to the case where only the FM core is used (for a distance $10d$) [compare (b),(c) and also (e),(f)].
2. The field that exists the hose in open geometries is non-uniform and the average field decreases respect to the corresponding closed cases [compare (a),(b) and (d),(e)].
3. When an open hose is ramified the output field in each branch decreases compared with the non-ramified case. However, the total average output field (adding up the field of all branches) is larger, similarly to what happens in closed geometries when branches are connected in parallel [compare (b) and (e)].
4. In open ramified hoses, the average output field in each branch can be different and depends on the distance between the branch end and the dipole source [see (e)].
5. When any of the branches of a ramified hose is closed (by a SC layer), the output field in the rest increases as if this branch was not present [compare (e), (g) and (h)].

- [1] Pendry, J. B., Schurig, D., and Smith, D. R. Controlling electromagnetic fields. *Science* **312**, 1780 (2006).
- [2] Cui, T.J., Smith, D.R. and Liu, R. Metamaterials: Theory, Design, and Applications. *Springer* (2010).
- [3] Cheng,Q. Study of three-dimensional optical-transformation devices based on analytical field-transformation theory. *Microwave and Millimeter Wave Technology (ICMWT), 2010 International Conference on.* 2082-2084 (2010).
- [4] Y. Levin and F. B. Rizzato. Superconducting pipes and levitating magnets. *Phys. Rev. E* **74**, 066605 (2006).